

A DUAL-POLARIZATION INVESTIGATION OF TORNADO-WARNED CELLS ASSOCIATED WITH HURRICANE RITA (2005)

CHRISTINA C. CROWE*⁺, WALTER A. PETERSEN[^], LAWRENCE D. CAREY[†], DANIEL J. CECIL[†]

⁺National Weather Service, Springfield, Missouri

[^]NASA Marshall Spaceflight Center, Huntsville, Alabama

[†]University of Alabama in Huntsville, Huntsville, Alabama

(Manuscript received 28 May 2010; in final form 23 August 2010)

ABSTRACT

Warning operations during hurricane events have been known to be particularly difficult when trying to determine the tornadic potential of cells within tropical cyclone (TC) rainbands. The Hurricane Rita (2005) tornado outbreak proved to be especially challenging for National Weather Service forecast offices in Mississippi and Alabama. A dual-polarization radar analysis of three mini-supercells was performed in order to investigate microphysical processes occurring within the cells. These three tornado-warned cells in the Huntsville, AL, County Warning Area (CWA) were chosen to represent one of each category: tornadic, funnel-producing, non-funnel producing. A comparison among these storms and to previous dual-polarimetric studies of tornadic supercells (non-tropical) was done to discern potential tornadic indicators that would help forecasters in warning operations. It has been found that while standard reflectivity features are quite different in tropical environments than in Midwest tornado outbreaks, dual-polarimetric radar features are similar in both instances. A distinct separation in specific differential phase and differential reflectivity (ZDR) can be seen in the tornadic case in addition to a clear ZDR arc. These observations suggest a different size sorting process due to a collapsing updraft and increased storm relative helicity associated with the tornadic storms.

1. Introduction

Hurricane Rita, which was part of a very active 2005 hurricane season, spurred one of the largest evacuations in U.S. history with possibly over two million evacuees from Texas alone (Beven et al. 2008). The focus of this study is on the tornado outbreak associated with Hurricane Rita as it moved inland.

*Corresponding author address: Christina C. Crowe, 5805 West Highway EE, Springfield, MO 65802
E-mail: Christina.Crowe@noaa.gov

One hundred and three tornadoes associated with Rita were reported across the Southeast between her landfall (24 Sept 2005) and transition to extra-tropical cyclone (26 Sept 2005) (NCDC, 2009). Throughout this event, the National Weather Service offices across the Southeast issued a total of 533 warnings with a Probability of Detection (POD) of 0.87 and False Alarm Ratio (FAR) of 0.84. Each Fiscal Year, the National Weather Service determines its goals for warning operations in terms of FAR, POD, and Lead Time. While not usually used as a yardstick for single events, but rather a year, this gives an indication of WFO performance. For the year of 2005, those goals were $FAR \leq 0.73$, $POD \geq 0.73$, and Lead Time = 13 minutes (DOC 2006). As radars nationwide begin to be upgraded to dual-polarimetric capabilities, this study hopes to identify key signatures for forecasters to use in the discrimination between tornadic and non-tornadic cells and therefore help reduce FAR in the future.

2. Previous dual-polarimetric radar studies

A handful of studies have investigated microphysical processes relevant to tornadogenesis and tornado potential in supercells from a research perspective using the evolution of dual-polarimetric (hereafter “dual-pol”) radar signatures (Kumjian and Ryzhkov (hereafter KR) 2007, KR 2008, KR 2009, Romine et al. 2008). The three main variables discussed in the literature and analyzed in this paper include horizontal reflectivity (Z_H), differential reflectivity (Z_{DR}) and specific differential phase (K_{DP}). Stated simply, Z_{DR} is the ratio of reflectivity at the horizontal (Z_H) and vertical (Z_V) polarizations, and gives reflectivity-weighted information about median drop size and shape. K_{DP} measures propagation properties of the scatterers across the radar cross section and hence indicates the size and concentration of

liquid hydrometeors. Typical ranges for most hydrometeors in C-band radar of Z_{DR} and K_{DP} are -2 dB to 6 dB and $-1^{\circ} \text{ km}^{-1}$ to $6^{\circ} \text{ km}^{-1}$, respectively. For further descriptions of the interpretation of these dual-pol variables, see Bringi and Chandrasekar (2001) or Straka et. al (2000).

A number of recent studies (Romine et al. 2008 and KR 2008, 2009) have identified a “ Z_{DR} arc” signature, in the lowest 1 km above ground level (AGL), associated with both tornadic and non-tornadic supercells. This signature occurs on the inflow side of cells along the Z_H gradient associated with the forward flank precipitation shield and often has Z_{DR} values greater than +5 dB, with values greater than +6 dB in tornadic cases (KR 2008). This enhanced Z_{DR} signature indicates the presence of larger raindrops outside of the core updraft of the cell. The arc shape to this enhanced Z_{DR} has only been noted in severe storms and may be evidence of a veering of the winds with height. Therefore, a Z_{DR} arc may also be an indicator of the strength of storm-relative helicity (SRH) (KR 2007, 2009).

Due to spatial variability in updraft strength and the vertical profile of storm-relative winds, size sorting of raindrops occurs in the horizontal. Smaller raindrops, which take longer to fall, are advected further downwind in the cell. Larger drops, unable to be suspended in weaker updrafts, are able to fall just outside of the updraft core (KR 2007, 2008). The result of this size sorting process is an enhancement in Z_{DR} along the right flank of the cell during its mature phase, while increased K_{DP} values appear in the higher liquid water content regions in the forward flank of the cell and deeper into the forward flank precipitation shield than the Z_{DR} arc ([Fig. 1](#)).

KR (2009) performed a modeling study to test the resulting dual-pol fields associated with variations in vertical wind shear. It was found that increased size sorting occurs in the horizontal as storm-relative wind speeds and directional shear increase. However, unidirectional shear in the environment of their modeled cells only led to Z_{DR} enhancements, not the arc shape,

which should be located along the inflow side of the cell along the reflectivity gradient associated with the forward flank downdraft, parallel to storm motion. When directional shear was added to the environmental profile, a Z_{DR} arc formed, with a positive correlation between increased directional shear and more substantial Z_{DR} values. Therefore it has been suggested that localized enhancements of SRH can be identified by increased Z_{DR} values in the arc.

3. Data and methodology

The radar used for this study was the ARMOR (Advanced Radar for Meteorological and Operational Research), which is located at the Huntsville International Airport. Further specifications for this C-band radar were discussed by Petersen et al. (2005, 2007). During the period of the study, ARMOR's scan strategy was set at RAIN1 which performs scans at three elevation angles: 0.7° , 1.3° and 2° . During this event new volume scans were available every 2 minutes. The beam width for this radar is 1.0° and range gate spacing is averaged to 250m from 125m during RAIN1 scans. ARMOR retrieves information on numerous single- and dual-polarization variables, but those discussed in this study include Z_H , v_r (radial velocity), Z_{DR} , and K_{DP} . Readers should bear in mind that specific values of Z_{DR} and K_{DP} presented in this paper cannot be directly transferred to WSR-88D dual-pol radar data, as both parameters are frequency dependent.

The data were edited with the NCAR SOLOII software. After the editing was performed, the data were gridded with a Cressman weighting function to a three-dimensional Cartesian grid, centered on the ARMOR radar location (1 km horizontal spacing). Constant-altitude plan

position indicators (CAPPIs) were produced for 6 levels with a resolution of every 1 km in the vertical. Time-height plots were also created for each cell lifecycle.

4. Analysis

An analysis of the 19 tornado warnings issued by WFO HUN during the course of the Hurricane Rita outbreak and associated tornado reports from NCDC (2009) was performed to identify cells of interest. It was determined that three particular cells traversed close enough (within 50km) to ARMOR to provide detailed analysis of the lower levels ([Fig. 2](#)). The initial cell of interest (Cell 15) prompted three warnings: 2012 UTC (Cullman Co), 2019 UTC (Morgan Co.) and 2041 UTC (Madison Co.). A F0 tornado was reported in Cullman Co. at 2018 UTC and a funnel cloud was reported in Morgan County at 2030 UTC. The second cell of interest (Cell 8) was associated with two tornado warnings for Limestone Co. (2100 UTC and 2127 UTC). The only report during this period was for a funnel cloud report Limestone Co. at 2115 UTC. The last cell of interest (Cell 16) was associated with a total of three tornado warnings: 2117 UTC (Cullman Co.), 2139 UTC and 2216 UTC (Morgan Co.). No funnel or tornado reports were associated with this cell.

4a. Tornadoic Cell

Cell 15 showed an organized structure as it developed into a mature supercell. Through the development into the mature phase of the storm, a distinct separation of Z_{DR} and K_{DP} maxima was observed ([Fig. 3](#)). As seen in the animation ([Fig. 4](#)), the K_{DP} was maximized in the forward flank of the storm, downshear of the main updraft of the storm. Meanwhile, the Z_{DR} maximized

on the right rear of the cell and wrapped around the back side of the updraft with maximum values approaching 8 dB and around 6 dB at the time of the tornado. These two characteristics of the K_{DP} and Z_{DR} maxima reflect the size sorting associated with the presence of a strong mesocyclone development shown in Fig. 3. Just prior to the tornado report in Cullman County, the occlusion of the mesocyclone and collapse of the updraft associated with the cell is indicated by an increase in the inflow notch and the erosion of the v-notch signature in the forward flank.

After the time of the tornado (2018 UTC), there was a Z_H increase in the storm's lower levels (1km) ([Fig. 5 and 6](#)) and the maximum became collocated with the relative K_{DP} and Z_{DR} maxima ([Fig. 7](#)). The Z_H increase began at 2014 UTC, just prior to the tornado report, and lasted through 2024 UTC, with an increase of 6 dBZ. While not a large difference in reflectivity, the maximum reflectivity had been fairly steady state for the 30 minutes prior. This sudden increase in low-level reflectivity suggests that updraft in the storm was beginning to collapse. With a collapsing updraft, larger raindrops would be able to fall to the surface, increasing the Z_H . The size-sorting previously provided by the mesocyclone would also weaken, as evidenced by the lack of separation between K_{DP} and Z_{DR} . The Z_H increase associated with the collapsing updraft and resultant tornadogenesis has also been noted by Romine et al. (2008) and KR (2008).

4b. Funnel Cloud Cell

Cell 8 exhibited a more linear structure than Cell 15. The polarimetric variables and radial velocity at the time of the funnel report (2115 UTC) in Limestone County ([Fig. 8](#)) showed only a slight Z_{DR} preference to the right rear of the storm. Additionally, there was slightly more overlap between K_{DP} and Z_{DR} maxima both at 2115 UTC and over the lifetime of the storm relative to Cell 15 as seen in the animation ([Fig. 9](#)). Weaker vertical shear than in the Cell 15

may be occurring at the time of the funnel cloud since there is less separation between these maxima. In addition, Z_{DR} values for the Limestone cell remain below 5 dB with only a slight increase from 3 to 4 dB around 2115 UTC. The lower Z_{DR} values indicate a weaker updraft that was unable to generate as large of raindrops as Cell 15. Strengthening or weakening of the updraft cannot be inferred around the time of the funnel report, as maximum Z_H values remained fairly consistent over a thirty minute period surrounding the funnel report.

Cell 16 had a structure similar to Cell 15 in that it had a more discrete supercellular type structure in Z_H , but the polarimetric structure was vastly different. As shown in the animation ([Fig. 10](#)), this cell appeared to undergo less sorting of drop size distribution and therefore less horizontal separation of the K_{DP} , Z_{DR} , and Z_H maxima. At the time of the second warning issued for the storm ([Fig. 11](#)), a slight v-notch was evident in the reflectivity, indicating a strong updraft. Velocity values indicated a strong mesocyclone, which likely prompted the warning. But while a marginal preference for larger drops and water-coated hail (greater K_{DP} , Z_{DR} , and Z_H) towards the right flank of the storm could be seen, there were overlapping bulls-eyes of all three values over the same region. Z_{DR} values around this time were not as high as near the Cell 15 tornado report, but still hovered around 5 dB.

Differences in size sorting can be seen among these cells. As evidenced by more overlap of K_{DP} , Z_{DR} , and Z_H for Cells 8 and 16 compared to Cell 15, size sorting through lofting smaller drops further downwind was unable to occur. Additionally, the Z_{DR} maximum was pushed further downwind of the core as compared to Cell 15, which suggests that large and small drops alike are being pushed equally far from the core. One explanation for this difference in size sorting could be that vertical shear was weaker than in Cell 15 (KR 2008). While other size

sorting processes could be responsible, these indicators may also suggest that a difference in vertical structure of tornadic storms could be the key to detection.

To summarize these dual-pol analyses, each of these cells was compared and contrasted to the fields observed by Romine et al. (2008) ([Fig. 1](#)). Each of the cells was analyzed around warning and tornado report times and simplified images comparable to the Romine figure were created ([Fig. 7, 12-13](#)). In the case of a tornadic cell, Cell 15, a separation of Z_{DR} and K_{DP} values occurred, with high Z_{DR} being located preferentially towards the right rear of the storm ([Fig. 3](#)). The Z_{DR} arc became more separated from the K_{DP} maximum and shifted further to the right rear along the Z_H gradient approaching and at the time of the tornado (2005 and 2017 UTC respectively). In addition, the arcing shape, as opposed to the more linear structure to the enhanced region of Z_{DR} in Cell 8 ([Fig. 12](#)), suggests that greater SRH (KR 2009) likely occurred in the near-storm environment of Cell 15. Conversely Cell 8 was moving into a more unidirectional speed shear region identified in the BNA sounding. Cell 15 also shows greater horizontal separation between the Z_{DR} and K_{DP} regions than did Cell 16 ([Fig. 13](#)).

When analyzing these general figures, it should be noted that comparing Z_H contour shape to that of the Romine image will likely hinder an understanding of this dual-pol analysis. The reader should keep in mind that cases studied in the referenced papers are associated with classic Great Plains style structure with an obvious hook or appendage signature. Because supercells associated with tropical cyclones are smaller, these signatures are less often sampled by radars, which contributes to the difficulty in making warning decisions with these cases. Since the dual-pol fields are similar to those seen in the classic cases even while their basic reflectivity patterns are not, this may reinforce the utility of dual-pol analysis in TC tornado cases. It should also be noted that even the modeling studies referenced in this paper have not

fully taken into account a detailed understanding of microphysical processes occurring in these storms (KR 2009). It would be beneficial in the future to perform a study that would analyze precipitation processes and drop trajectories using a Lagrangian framework.

5. Summary and conclusions

Hurricane Rita's tornadoes provided a significant challenge to forecasters at the National Weather Service, including those in north central Alabama. While not unusual for landfalling TC cases, which are notoriously difficult warning situations, the verification statistics from this case lead to inquiries about what could be done with technologies that will be available in the near future to improve upon warning capabilities.

From the three cells investigated in northern Alabama, differences in the microphysical processes occurring within each storm can be identified through dual-pol analysis. In the storm that produced the tornado in Cullman County (Cell 15), a horizontal displacement of the maximum Z_{DR} and K_{DP} values suggests size sorting of hydrometeors due to a stronger updraft that begins to collapse in addition to increased directional shear within the storm. The other two non-tornadic storms display more co-located maxima of Z_{DR} and K_{DP} and smaller changes in Z_H over time which indicates a lack of significant updraft strengthening or collapse. These findings agree with previous dual-pol studies on tornadic storms.

Of the few previous distinctions made between tornadic and non-tornadic cells, KR's (2008) determination that Z_{DR} values of greater than 6 dB were associated with tornadic cells also holds in our Hurricane Rita cells studied, with the tornadic cell consistently at or above this value. The tornadic storm also exhibits Z_{DR} being wrapped around the back side of the updraft,

which agrees with previous observations of Z_{DR} being pulled into the hook (KR 2008), even though in this case no obvious hook is evident in the reflectivity field.

These findings suggest that warning operators can benefit from dual-pol technology that will be operational nationwide in the near future. The spatial separation of dual-pol values that suggest enhanced size sorting within tornadic supercells will likely be a useful indicator for forecasters. The fact that dual-pol fields are similar in tropical and Midwest tornadic cases will also aid forecasters who irregularly experience landfalling tropical cyclones.

It should be noted that this small dataset is not robust enough alone to draw statistically relevant conclusions on dual-pol differences between tornadic and non-tornadic cells. Further study of TC tornado cases should be undertaken including a comparison to cold season tornadoes in similar high shear and low CAPE environments in northern Alabama, as well as other dual-pol studies. The suggestion of an ideal range for Z_{DR} (KR 2008b) should also be studied for the larger dataset that is partitioned by wavelength (e.g., C-band and S-band). Through further investigation of these storms, polarimetric signatures and distinctions between tornadic and non-tornadic cells can hopefully be identified to aid the operational community.

Acknowledgements. This work was supported by a Graduate Fellowship from the American Meteorological Society while the lead author completed graduate work at the University of Alabama in Huntsville. The authors would like to recognize funding from NOAA for the UAH THOR Center. WAP also acknowledges funding support from Dr. Ramesh Kakar of the NASA Precipitation Science Program. Special thanks to Mr. Michael Coyne and the staff of the National Weather Service in Huntsville, Alabama, and Dr. Kevin Knupp, Cody Kirkpatrick,

Elise Johnson and Lori Schultz at the University of Alabama in Huntsville for help in completing this research.

REFERENCES

- Beven, J.L. II, L.A. Avila, E.S. Blake, D.P. Brown, J.L. Franklin, R.D. Knabb, R.J. Pasch, J.R. Rhome, and S.R. Stewart, 2008: Annual summary: Atlantic hurricane season of 2005. *Mon. Wea. Rev.*, **136**, 1109-1173.
- Bringi, V.N. and V. Chandrasekar, 2001: The Polarimetric basis for characterizing precipitation. *Polarimetric Doppler Weather Radar: Principles and Applications*. Cambridge University Press, 378-532.
- DOC, 2006: U.S. Department of Commerce Performance and Accountability Report for FY2005. www.osec.doc.gov/bmi/budget/05APPR/PAR05.pdf, 290.
- Kumjian, M.R., and A. Ryzhkov, 2007: Polarimetric characteristics of tornadic and nontornadic supercell thunderstorms. Preprints, *33rd Conference on Radar Meteorology*, Cairns, Queensland, Ameri. Meteor. Soc., CD-ROM, P10.1.
- , and -----, 2008: Polarimetric signatures in supercell thunderstorms. *J. Appl. Meteor.*, **47**, 1940-1961.
- , and -----, 2008b: Microphysical differences between tornadic and nontornadic supercell rear-flank downdrafts revealed by dual-polarization radar measurements. Preprints, *24th Conference on Severe Local Storms*, Savannah, Georgia, Ameri. Meteor. Soc., CD-ROM, 3B.4.

- , and -----, 2009: Storm-relative helicity revealed from polarimetric radar measurements. *J. Atmos. Sci.*, **66**, 667-685.
- Markowski, P.M., J.M. Straka, and E.N. Rasmussen, 2002: Direct surface thermodynamic observations within the rear-flank downdrafts of nontornadic and tornadic supercells. *Mon. Wea. Rev.*, **130**, 1692-1721.
- NCDC (National Climatic Data Center), cited 2009: NCDC Storm Events Database. [Available online at <http://www4.ncdc.noaa.gov/cgi-win/wwcgi.dll?wwEvent~Storms>]
- Petersen, W.A., K. Knupp, J. Walters, W. Deierling, M. Gauthier, B. Dolan, J.P. Dice, D. Satterfield, C. Davis, R. Blakeslee, S. Goodman, S. Podgorney, J. Hall, M. Budge, and A. Wooten, 2005: The UAH-NSSTC/WHNT ARMOR C-band dual-polarimetric radar: A unique collaboration in research, education and technology transfer. Preprints, *32nd Conference on Radar Meteorology*, Albuquerque, New Mexico, Ameri. Meteor. Soc., CD-ROM, 12R.4.
- , K.R. Knupp, D.J. Cecil, and J.R. Mecikalski, 2007: The University of Alabama Huntsville THOR Center Instrumentation: Research and operational collaboration. Invited Presentation, *33rd International Conference on Radar Meteorology*, Ameri. Meteor. Soc., Cairns, Australia, August 6-10, 2007.
- Romine, G.S., D.W. Burgess, and R.B. Wilhelmson, 2008: A dual-polarization-radar-based assessment of the 8 May 2003 Oklahoma City area tornadic supercell. *Mon. Wea. Rev.*, **136**, 2849-2870.
- Straka J.M., D.S. Zrnic, A.V. Ryshkov, 2000: Bulk hydrometeor classification and quantification using polarimetric radar data: synthesis of relations. *J. Appl. Meteor.*, **39**, 1341-1372.

TABLES AND FIGURES

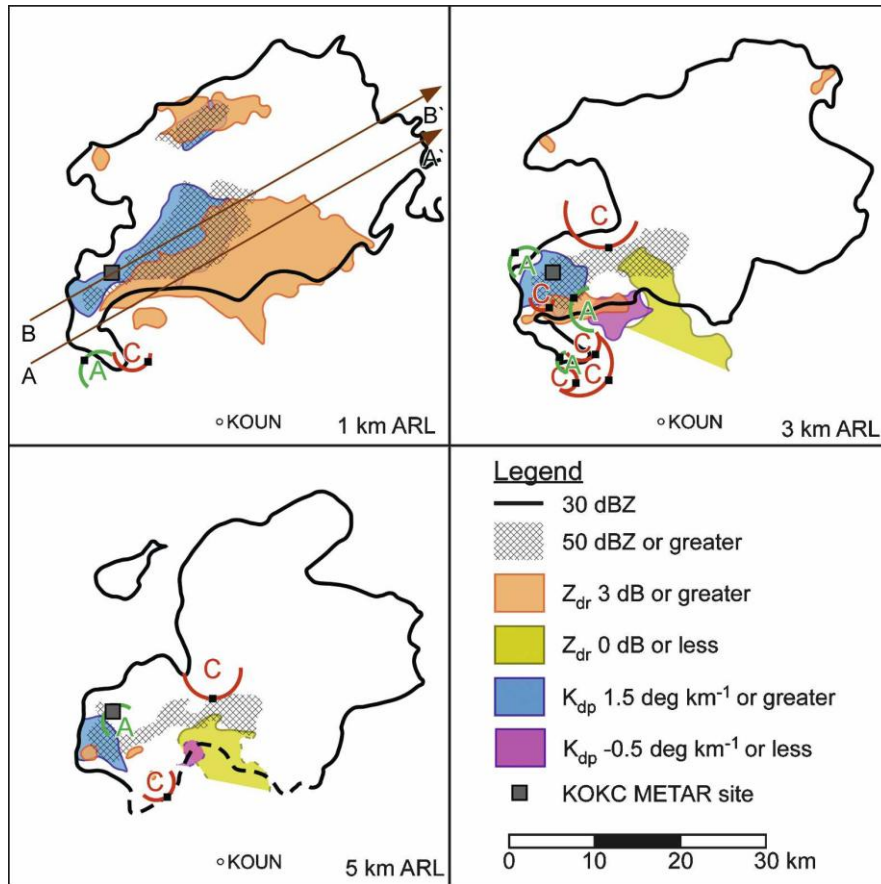


Figure 1. CAPPI plot at 1 km (top left), 3 km (top right) and 5 km (bottom left) ARL (above radar level) at 2204 UTC on 8 May 2003, near Oklahoma City, OK. Contours and shading done according to the inset legend. Half circles with the letter A indicate a region of anticyclonic rotation while half circles with the letter C indicate regions of cyclonic rotation. Small black boxes indicate couplet alignment relative to the radar. A tornado was reported at 2206 UTC (Figure 12 from Romine et al. 2008 – re-printed with the permission of the AMS).

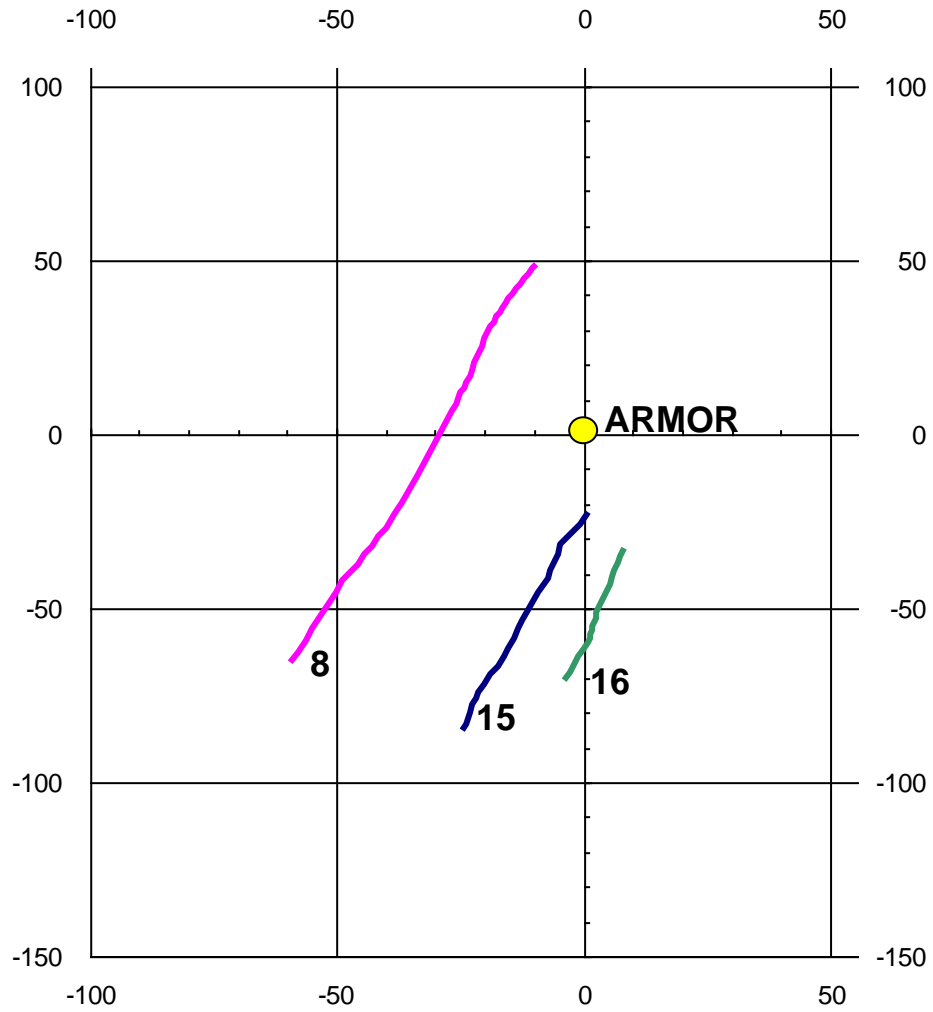


Figure 2. Track of three storms used for dual-pol study and the location of ARMOR. Grid units are in km.

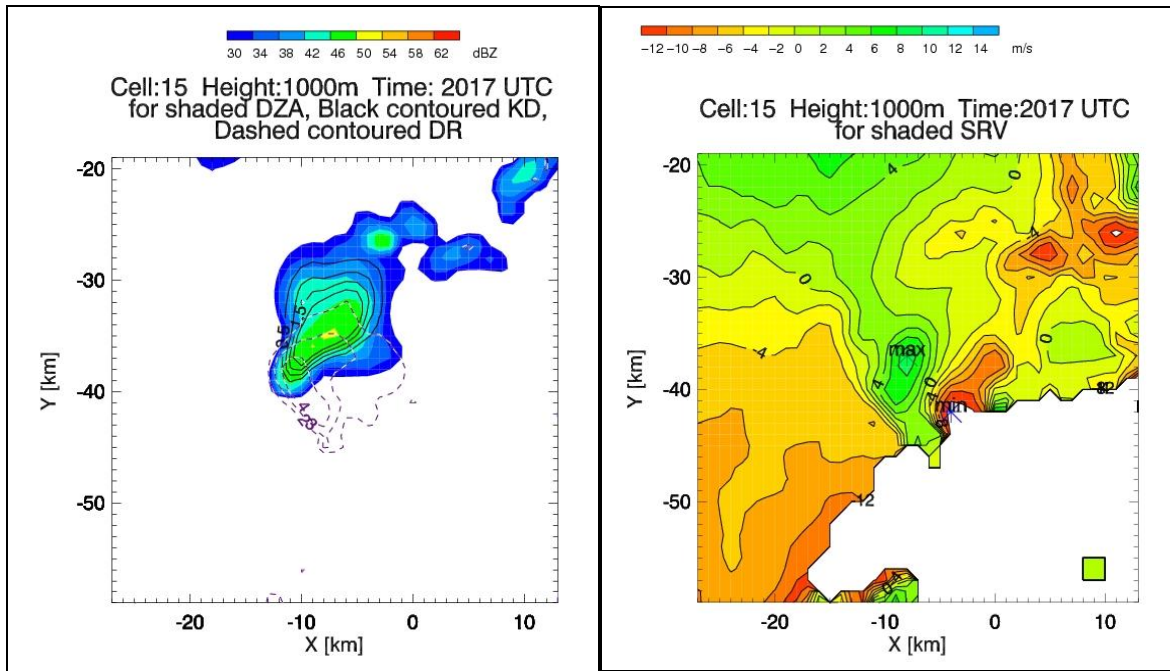


Figure 3. Radar polarimetric variables for Cell 15 at 2017 UTC 25 Sept., shown on a 1-km CAPPI: (a) reflectivity factor (Z_H ; dBZ) is shaded every 4 dBZ beginning at 30 dBZ, differential reflectivity (Z_{DR} ; dB) is dashed contoured every 1 dB from 2 – 5 dB, specific differential phase (K_{DP} ; $^{\circ} \text{ km}^{-1}$) is solid contoured every $0.5^{\circ} \text{ km}^{-1}$ from 0.5 to $2.0^{\circ} \text{ km}^{-1}$, and (b) storm relative Doppler velocity (SRV; m s^{-1}) is contoured and shaded every 2 m s^{-1} .

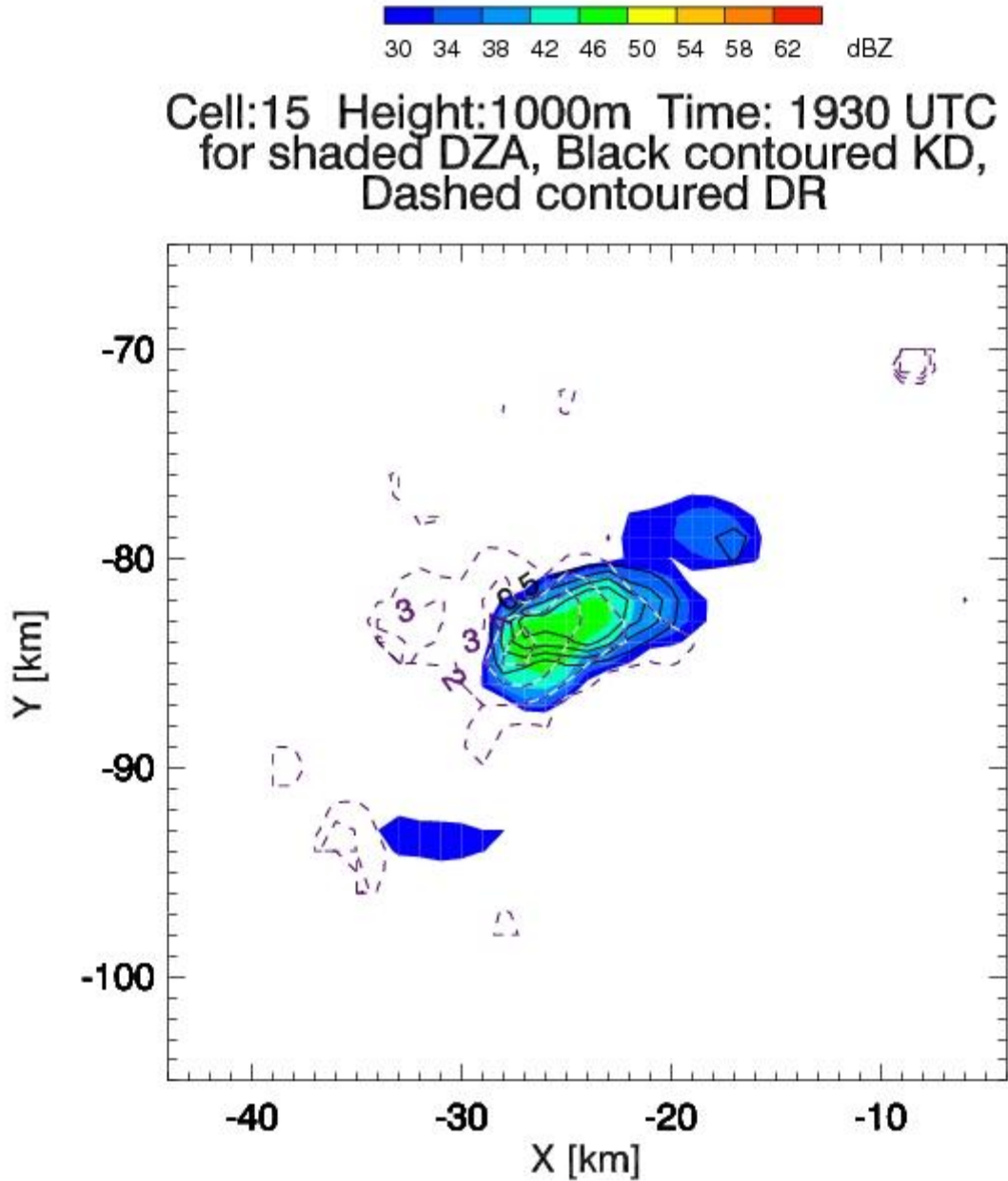


Figure 4. Animated loop of radar polarimetric variables for Cell 15 from 1930 to 2030 UTC 25 Sept., shown on a 1-km CAPPI: reflectivity factor (Z_H ; listed as DZA in image; dBZ) is shaded every 4 dBZ beginning at 30 dBZ, differential reflectivity (Z_{DR} ; listed as DR in image, dB) is dashed contoured every 1 dB from 2 – 5 dB, specific differential phase (K_{DP} ; listed as KD in image, $^{\circ} \text{ km}^{-1}$) is solid contoured every $0.5^{\circ} \text{ km}^{-1}$ from 0.5 to $2.0^{\circ} \text{ km}^{-1}$.

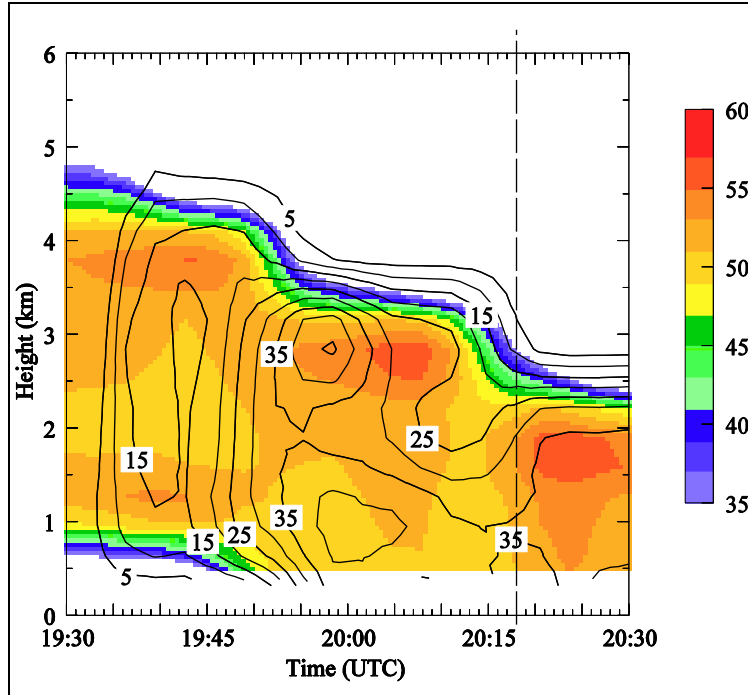


Figure 5. Time-height analysis for Cell 15 from 0.5 to 6 km of maximum reflectivity (dBZ – shaded from 35 – 60 dBZ according to color bar on right) and angular momentum ($\text{m s}^{-1} \text{ km}$ – contoured in black, not discussed here). Tornado time is indicated by the vertical dashed line. Missing data is left shaded white. Data from ARMOR radar was limited only to the lower levels and no data from other radars was available to supplement the upper level data. The gradient on the upper edge of the shading, therefore, is likely an artifact of missing data. Cell 15 is 89 km from ARMOR at the beginning of the period, is 60 km away at 2000 UTC, and is 23 km away at the end of the period.

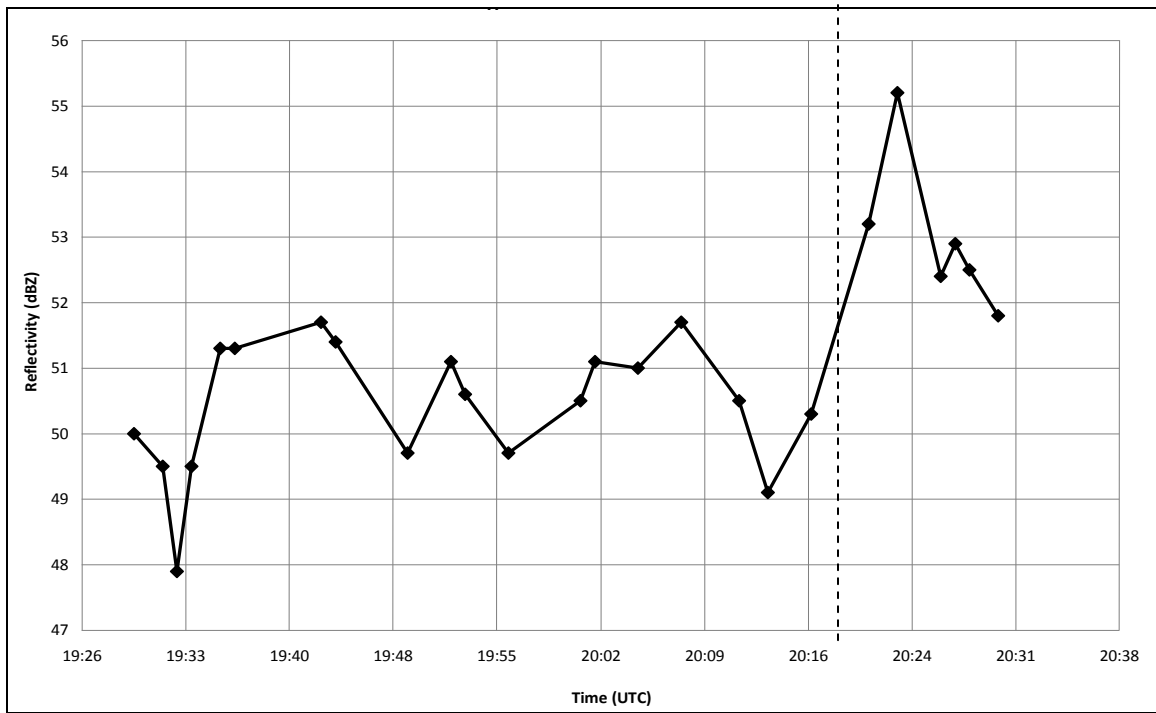


Figure 6. Trend of maximum reflectivity value in Cell 15 over time (in black) at 1km altitude. The dashed line indicates the time of the tornado report in Cullman County.

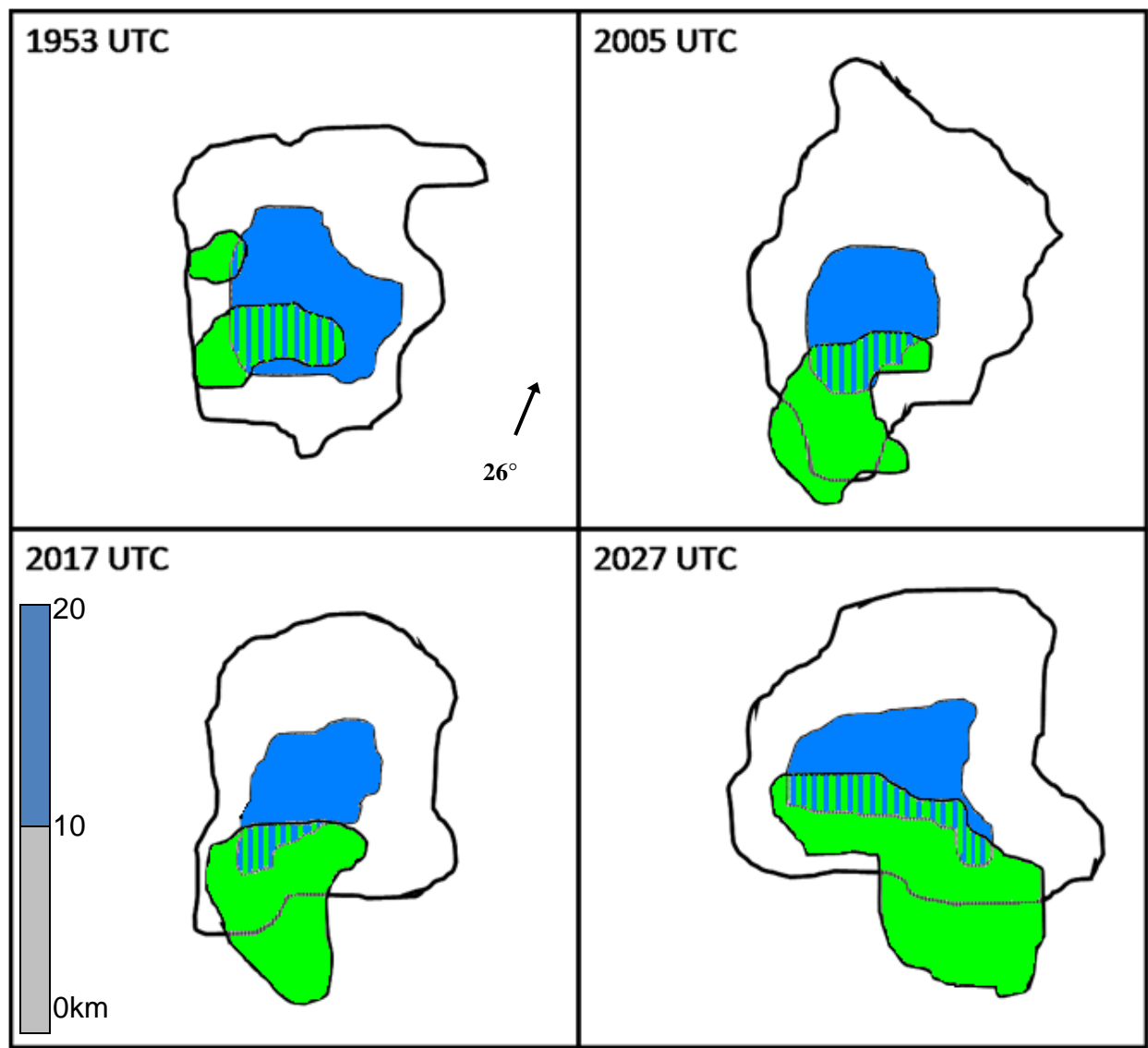


Figure 7. Time series for Cell 15 at 1953 UTC (top left), 2005 UTC (top right), 2017 UTC (bottom left), and 2027 UTC (bottom right) at a height of 1 km. The thick black line indicates the 30 dBZ reflectivity contour, the green filled region indicates differential reflectivity values greater than 3 dB, and blue shaded region indicates specific differential phase values greater than $1.5 \text{ }^{\circ}\text{km}^{-1}$. Direction of storm motion indicated by arrow in top left panel. The length scale is given in the bottom left panel in kilometers.

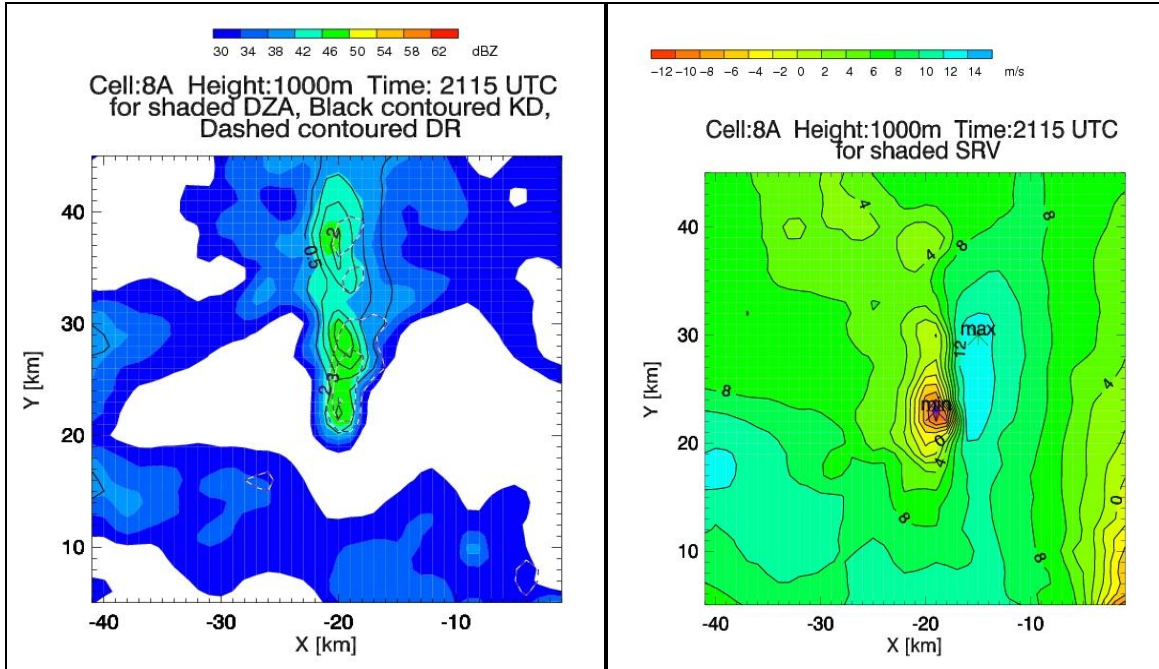


Figure 8. Same as Figure 3 except for Cell 8 at 2115 UTC 25 Sept. Here Z_H is listed as DZA, Z_{DR} is listed as DR, and K_{DP} is listed as KD.

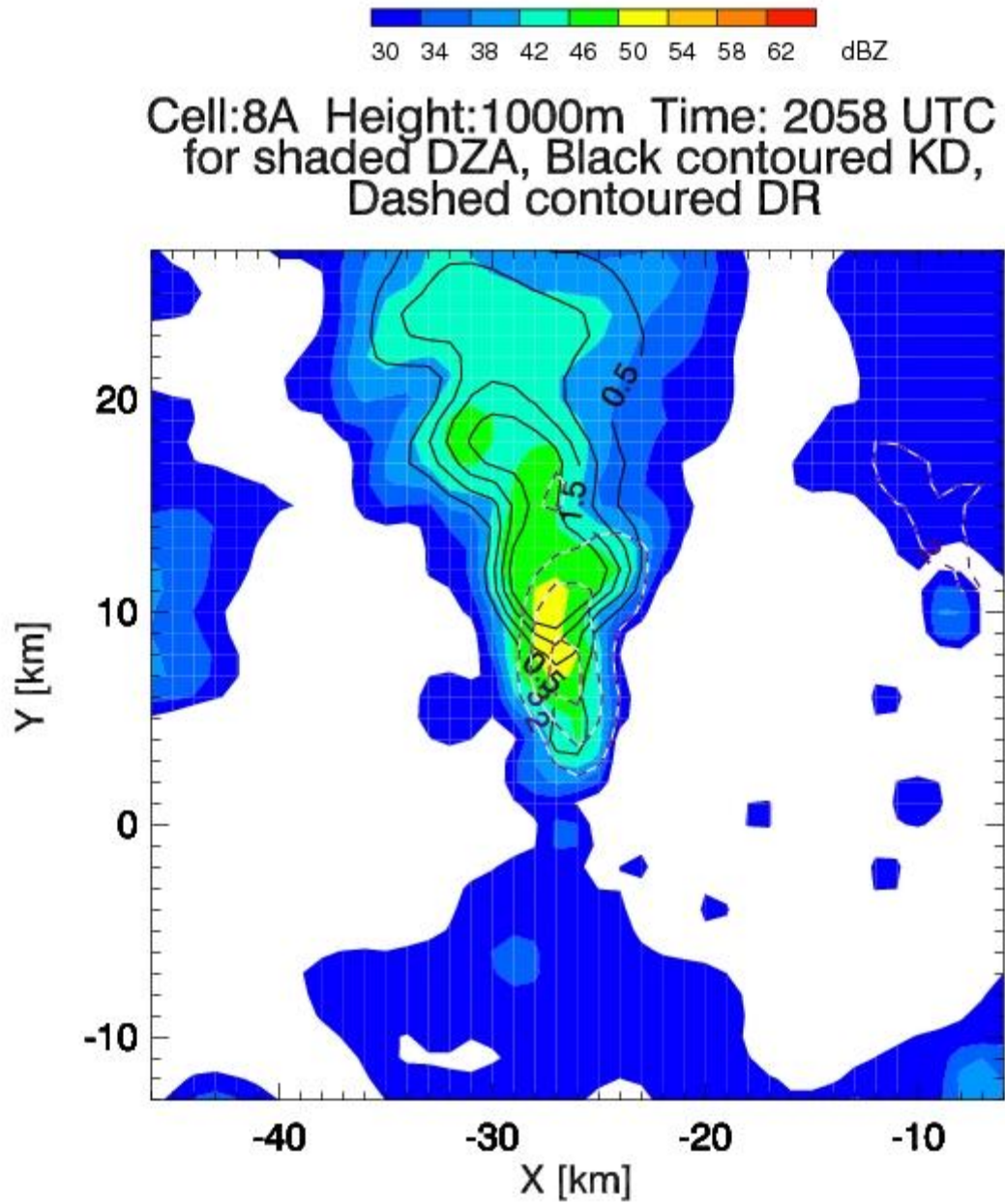


Figure 9. Animated loop of radar polarimetric variables for Cell 8 from 2058 to 2141 UTC 25 Sept., shown on a 1-km CAPPI. Shading is the same as in Figure 4.

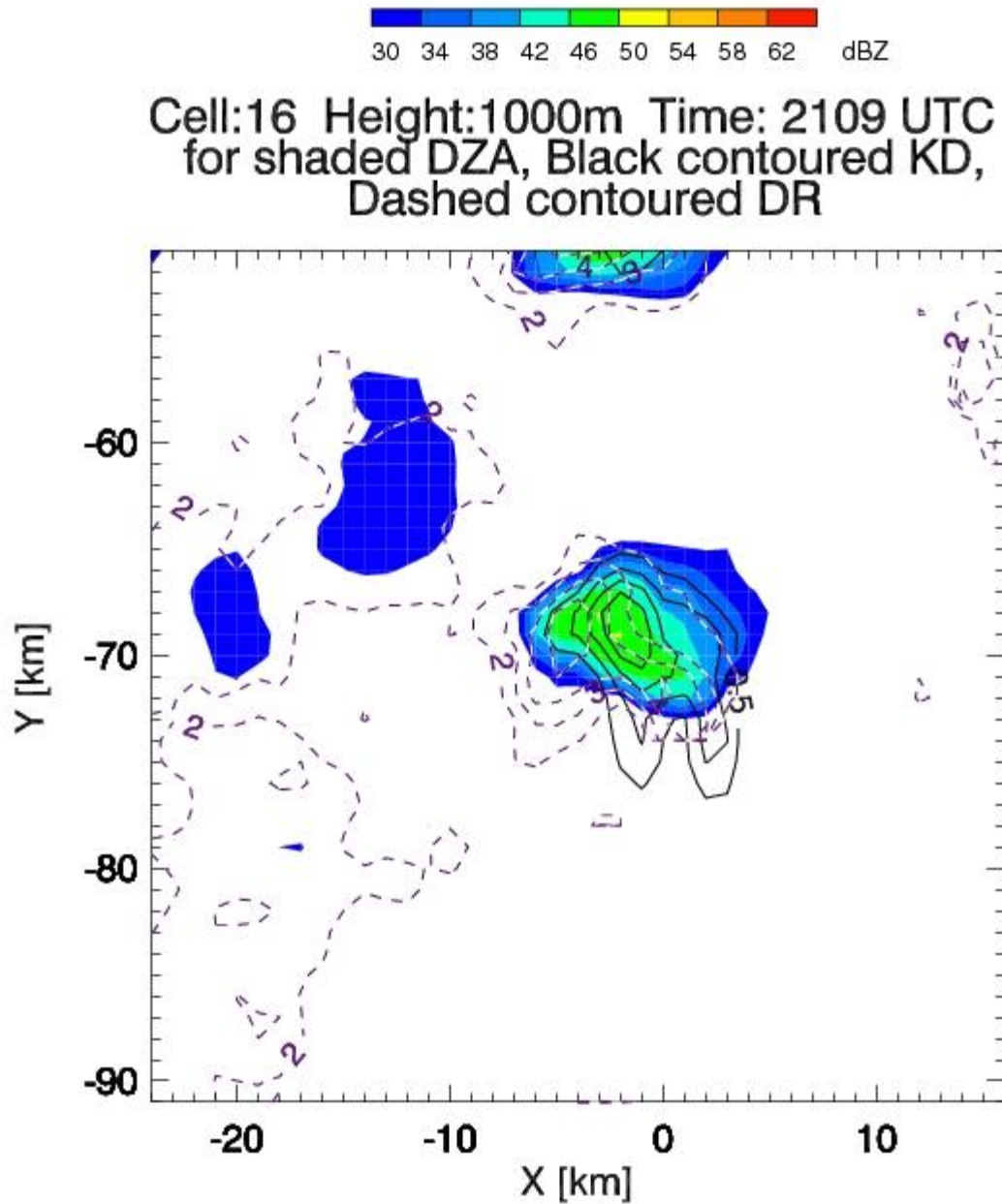


Figure 10. Animated loop of radar polarimetric variables for Cell 16 from 2109 to 2151 UTC 25 Sept., shown on a 1-km CAPPI. Shading is the same as in Figure 4.

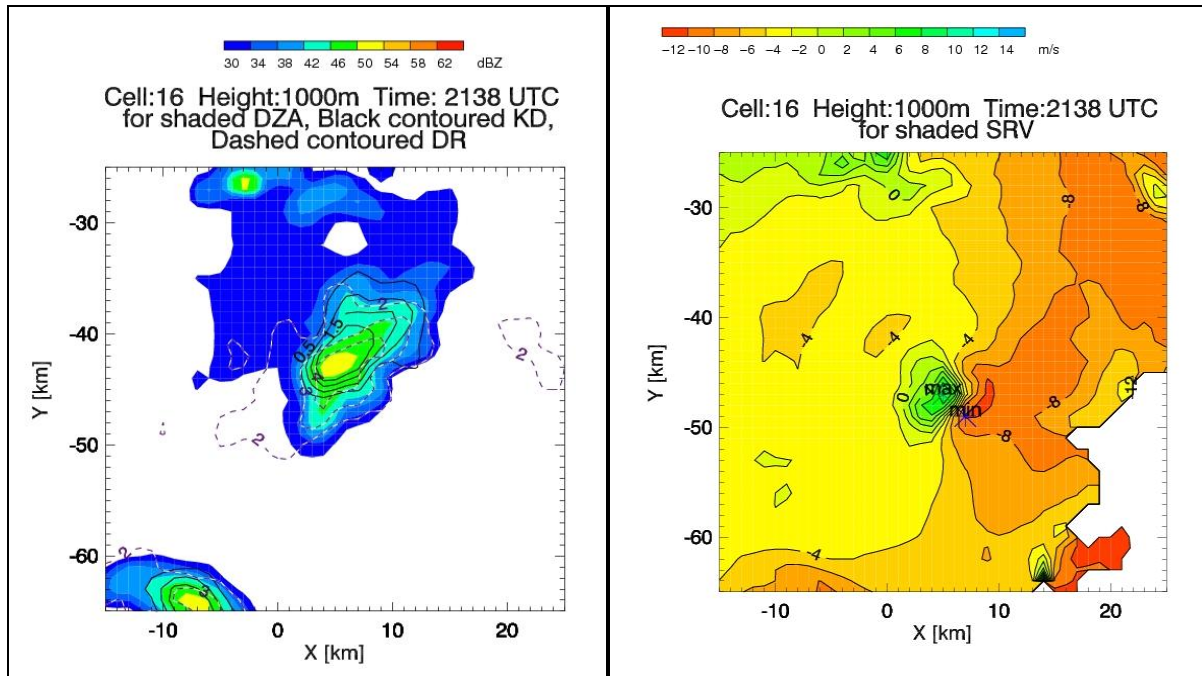


Figure 11. Same as Figure 3 except for Cell 16 at 2138 UTC 25 Sept. Here Z_H is listed as DZA, Z_{DR} is listed as DR, and K_{DP} is listed as KD.

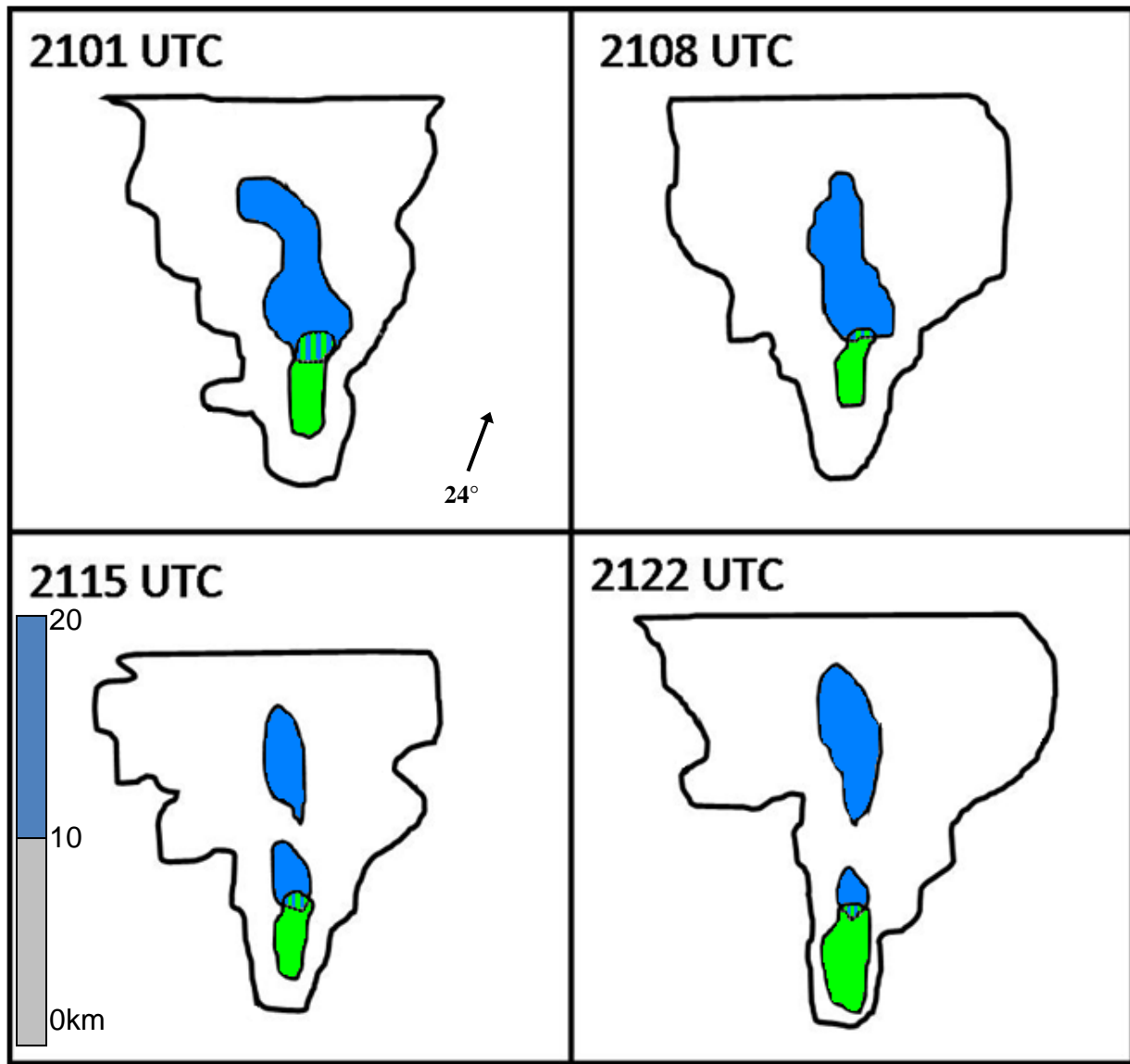


Figure 12. Time series for Cell 8 at 2101 UTC (top left), 2108 UTC (top right), 2115 UTC (bottom left), and 2122 UTC (bottom right) at a height of 1 km. Same shading as Figure 7.

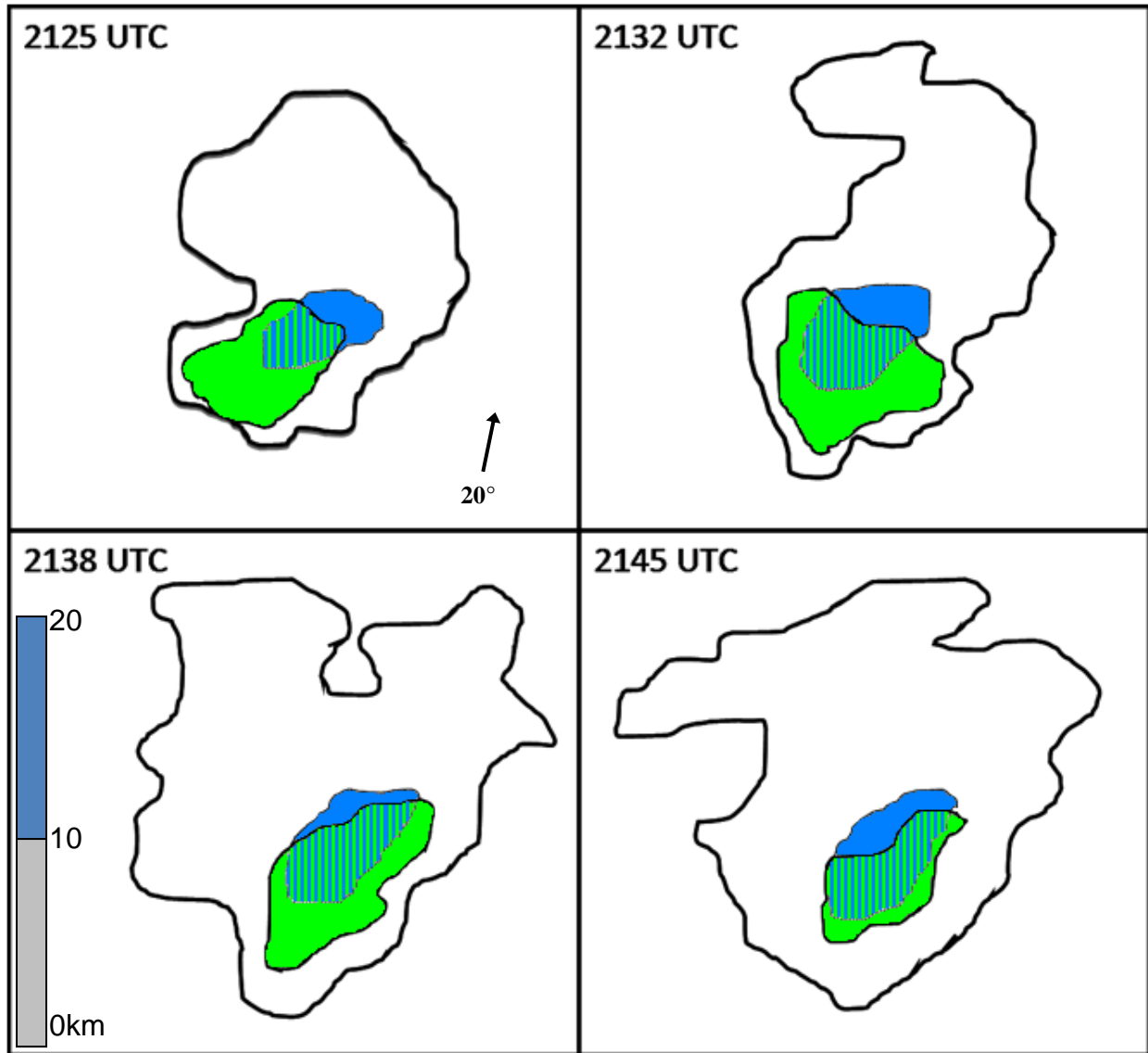


Figure 13. Time series for Cell 16 at 2125 UTC (top left), 2132 UTC (top right), 2138 UTC (bottom left), and 2145 UTC (bottom right) at a height of 1 km. Same shading as Figure 7.